Mechanical properties and thermal stability of ZrCuAlx thin film metallic glasses: Experiments and first-principle calculations

C. Poltronieri, A. Brognara, F. Bignoli, S. Evertz, P. Djemia, D. Faurie, F. Challali, C.H. Li, L. Belliard, G. Dehm, et al.

Mechanical properties and thermal stability of $ZrCuAl_x$ thin film metallic glasses: Experiments and first-principle calculations

C. Poltronieri[1], A. Brognara[2], F. Bignoli[1], S. Evertz[2], P. Djemia[1], D. Faurie[1], F. Challali[1], C.H. Li[3], L. Belliard[4], G. Dehm[2], J.P. Best[2], M. Ghidelli[1]

[1]Laboratoire des Sciences des Procédés et des Matériaux (LSPM), CNRS, Université Sorbonne Paris Nord, 93430, Villetaneuse, France

[2]Max-Planck-Institut für Eisenforschung GmbH, 40237 Düsseldorf, Germany

[3] State Key Laboratory of Superlattices and Microstructures, Institute of Semiconductors, Chinese Academy of Sciences, Beijing 100083, China

[4]Institut des NanoSciences de Paris, Sorbonne Université Paris, France

Keywords: Thin film metallic glasses; Mechanical properties; Thermal stability; Ab initio molecular dynamics; High-energy diffraction.

Abstract

In this work, we provide a holistic picture about the relationship between atomic structure, mechanical properties, and thermal stability of $ZrCuAl_X$ thin film metallic glasses (TFMGs) varying the Al content from 0 to 12 at.%, carrying out a broad characterization involving experiments and *ab initio* molecular dynamic simulations (AIMD). We show that the addition of Al resulted in a change of average interatomic distances by ~10 pm with the formation of shorter bonds (Al-Zr and Al-Cu), influencing the mechanical response (shear/elastic moduli and hardness) which increases by ~15% for 12 at.% Al. Moreover, tensile tests on polymer substrate revealed a maximum value for the crack initiation strain of 2.1% for $ZrCuAl_9$, while the strain-to-failure rapidly decreases at higher Al contents. The observed reduction in damage tolerance is correlated to a transition in atomic configuration. Specifically, a maximum in density of full and defective

icosahedral cluster population is observed at 9 at.% Al, inducing a more shear-resistant behavior to the material. Thermal stability is investigated by high-energy and conventional x-ray diffraction and electrical resistivity measurements as a function of the temperature. Glass transition (T_g) and crystallization (T_x) temperature increase by Al addition reaching 450 and 500 °C, respectively for $ZrCuAl_{12}$. The increase in thermal stability is related to the reduction in atomic mobility due to the formation of shorter chemical bonds, inhibiting atomic reconfiguration during crystallization. In conclusion, we provide guidelines to the design of compositional-tailored $ZrCuAl_x$ TFMGs with tuned mechanical properties and thermal stability with potential impact on industrial applications.

1. Introduction

Bulk metallic glasses (BMGs) are characterized by a disordered atomic structure that leads to high elastic deformations (>2%) and yield strength (~2 GPa) in combination with good corrosion and wear resistance, above those of most traditional crystalline materials [1, 2]. However, the absence of dislocations results in a macroscopically brittle behavior at T_{room} with the deformation entirely localized in narrow (~10 nm thick) shear bands (SBs) [3]. This brittle behavior can be mitigated by reducing the sample dimensions. Specifically, mechanical size effects can be activated for sub-micrometer scale samples hindering shear band nucleation and propagation as in the case of thin film metallic glasses (TFMGs), in which large plastic deformation and toughness are reported [4, 5]. As an example, in the case of 200-300 nm-thick ZrCu TFMGs deformed in tension, Tian *et al.* [6] found a fracture stress close to the theoretical limit (~3.5 GPa), while other studies also demonstrated the capability of TFMGs to deform plastically even reaching strains >10% with ductile necking [7-10].

Control over composition and microstructure play a primary role on the mechanical behavior of both bulk and TFMGs, as for Zr_xCu_{100-x} TFMGs [11, 12], making them promising candidates for the development of innovative stretchable electronic technologies [11, 13]. *Ab initio* modeling of MGs reveal that a low overall fraction of hybridized bonds is a selection criterion for proposing damage-tolerant metallic glass systems [14]. As determining the bonding characteristics is not trivial, simpler criteria are often used, such as the first-order

approximation by Lewandowsky *et al.* [15], which assumes that a high Poisson's ratio (>0.32) often indicates a high fracture energy and thus a tough and ductile material. As an example, the increase of Al content in $ZrCuAl_x$ BMGs was reported to improve the mechanical properties by both molecular dynamics studies [16] and experimental observations [17-19]. Specifically, in the case of $ZrCuAl_x$ BMGs, Yu *et al.* [17] revealed a maximum of Poisson's ratio (0.37) and plastic strain in compression (up to 16%) by adding 5 at.% Al. Moreover, Limbach *et al.* [18] showed that adding Al to ZrCu BMGs increases the shear and Young's moduli by 10% from 32 up to 36 GPa and from 100 to 115 GPa, respectively, for 8 at.% Al. Das *et al.* [19] compared compression tests on $Zr_{50}Cu_{50}$ and $Zr_{47.5}Cu_{47.5}Al_5$ BMGs and they observed that Al has a beneficial effect on the yield strength and strain to failure, which both increased from 1270 to 1550 MPa and 7.9 to 18%, respectively. They showed that the Al addition promotes structural inhomogeneity leading to the nucleation of multiple shear bands and increasing the flow stress necessary for failure [19].

Another interesting feature of ZrCu BMGs is the high thermal stability which can reach 390 °C for ~50 at.% Cu due to the minimum of formation enthalpy and maximum of configurational entropy stabilizing the amorphous structure [20, 21]. Moreover, the thermal stability can been related to the maximal population of highly symmetric and thermodynamically stable icosahedra hindering crystallization [22]. For the case of $ZrCuAl_x$ alloys, the thermal stability depends on the electronic structure and atomic bonding [23]. Generally, an electronegativity difference between the elements composing the material determines the stability of metallic compounds. Specifically, a low electronegativity difference is generally a fingerprint of a more dominant metallic-bond structure (than covalent one), which is known to increase the toughness of metallic glasses [24]. Numerical simulations performed with a reverse Monte Carlo method and combined with extended X-ray absorption fine structure (EXAFS) on $ZrCuAl_x$ BMG were used to investigate the chemical bonding [25, 26]. These studies showed that shorter Zr-Al bonds lengths lead to the formation of Al-centered clusters which can pin larger Zr-centered and Cu-centered clusters, reducing atomic mobility and then improving the thermal stability. Furthermore, the addition of Al and other elements (such as Ag, Ta, or Mo) for ternary and quaternary alloys showed a reduced possibility of phase segregation and further increase in the thermal stability of ZrCu-based metallic glasses [27-29].

It is thus clear that the addition of Al can play a significant role on mechanical properties and thermal stability of ZrCu-based MGs. However, a complete understanding of the relationship between atomic structure, mechanical properties and thermal stability in $ZrCuAl_x$ in thin film form (i.e. for TFMGs) has never been addressed, requiring a number of delicate experiments in combination with AIMD aiming to grasp the fundamental physical interconnects. Furthermore, only very limited data are available concerning more relevant (>10 at.%) additions of solute in ternary ZrCu-based systems, making the investigation of the atomic structure-mechanical properties-thermal stability relationship an open scientific domain.

In this study, the effect of Al addition on the atomic structure, mechanical behavior and thermal stability of $ZrCuAl_x$ TFMGs (x = 0, 6, 8, 9, 12 at.%) has been extensively analyzed through complimentary techniques such as scanning electron microscope/energy dispersive x-ray analysis (SEM/EDX), x-ray diffraction (XRD), high-energy synchrotron-source XRD (sXRD) (both carried out to 600 °C), nanoindentation, optoacoustic techniques, and tensile testing on polymeric substrates. The experimental results are compared with *ab initio* molecular dynamics simulations to gain insights on the local chemical order and bonding nature. Overall, we provide a holistic picture about the relationship atomic structure-mechanical properties-thermal stability for $ZrCuAl_x$ TFMGs, paving the way to compositional design of TFMGs with large thermal stability and mechanical resistance.

2. Experimental

2.1 Synthesis of $ZrCuAl_x$ TFMGs

$ZrCuAl_x$ TFMGs were deposited by magnetron (co)sputtering with three 99.99 at.% pure Zr, Cu and Al targets (Kurt J. Lesker®). The chamber base pressure was equal to 10^{-5} Pa, while the working pressure was set to 0.5 Pa with an Ar flow rate of 40 sccm at T_{room}. The power ratio between Zr and Cu targets was calibrated to obtain a $Zr_{50}Cu_{50}$ alloy, then the Al content was controlled by applying different powers from 10 up to 25 W, resulting in a tunable Al content from 0 up to 12 at.%. Films were deposited on Si (100), fused SiO_2, Si coated

with Si_3N_4 and Kapton® substrates, cleaned in an ultrasonic bath with isopropanol prior to use. For all samples, the thickness was fixed and equal to 800 ± 20 nm.

2.2 Structural and chemical characterization at T_{room}

A field emission scanning electron microscope (FE-SEM) Zeiss Supra 40 equipped with a Bruker energy dispersive X-ray spectroscopy (EDX) was used to perform morphological and elemental characterization of $ZrCuAl_x$ TFMGs deposited onto Si. X-ray diffraction (XRD) was used to analyze the structural evolution by using a RIGAKU SMARTLAB 9KW diffractometer with Cu-Kα radiation (~8 keV, λ = 1.5406 Å) in Bragg–Brentano geometry.

2.3 Evolution of the atomic structure and devitrification phenomena by synchrotron-source XRD

Synchrotron X-ray diffraction (sXRD) was carried out to unravel the fine atomic structure and the devitrification phenomena of $ZrCuAl_x$ TFMGs. High-energy (~100 keV, λ = 0.12224 Å) diffraction measurements were performed at the PETRA III P21.1 beamline at the Deutsches Elektronen-Synchrotron (DESY, Hamburg). The $ZrCuAl_x$ TFMGs were deposited onto specifically designed fused silica substrates (**Fig. 1**). The substrates had a thickness of ~2 mm, which was reduced in the central part down to a thickness <100 µm through a laser-milled window of 2 mm of diameter (**Fig. 1**, supplied by Schröder Spezialglas GmbH, Germany). Prior to annealing, the vacuum chamber was evacuated down to a base pressure of $5 \cdot 10^{-4}$ mbar. The structural evolution as a function of temperature was investigated by *in situ* heating from T_{room} up to 150 °C with a ceramic heating element from Bach and linear heating ramp of 10 K/min. Successively, the temperature was kept constant for 3 minutes each 10 °C upon reaching of 600 °C, in order to observe the crystallization phenomena. The same thermal history was also applied to a bare SiO_2 substrate to perform an accurate background subtraction. Diffraction patterns (~20s collection time) were recorded continuously during the heating protocol. A Perkin Elmer XRD1621 fast detector was utilized at a distance of ~1.5 m. The collected 2D diffraction patterns were integrated using the pyFAI package, resulting in intensity *I(Q)* which was then processed using PDFgetX3 enabling the determination of the structure function *S(Q)* and the pair distribution function *G(r)*.

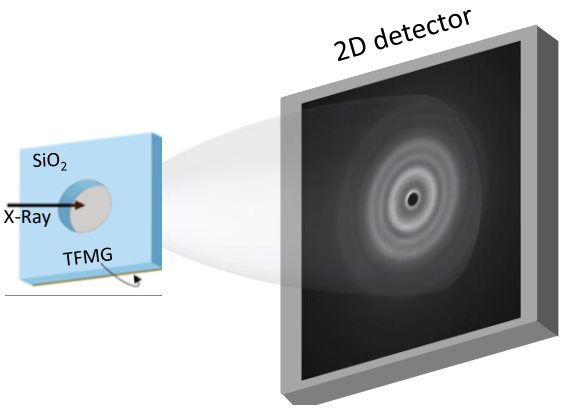

Fig. 1: Schematic of the sXRD setup used to analyze the atomic structure and devitrification phenomena of $ZrCuAl_x$ TFMGs.

2.4 Thermal stability of $ZrCuAl_x$ TFMGs (XRD and electrical resistivity measurements)

In addition to sXRD, a macroscopic analysis of thermal stability and devitrification processes has been carried out by X-ray diffraction (XRD) and electrical resistivity measurements as a function of temperature. In both cases, TFMGs were deposited onto Si wafer coated with Si_3N_4 to avoid interface diffusion. The diffractometer was coupled with an Anton Paar DHS 1100 system designed for *in situ* heating in He atmosphere (1.35 bar). The sample were fixed on an AlN plate and heated from room temperature up to 600 °C with a heating rate of 30 °C/min. Diffractograms were acquired at constant temperatures every 30 °C, within the 25–90° 2θ range in continuous mode and with acquisition time of 22 min.

The electrical resistivity measurements were carried out from T_{room} up to 540 °C with a Van der Pauw configuration [30]. The films were held in a LINKAM - HFS600 probing system consisting of 4 tungsten needles as electrical contacts. The system was heated under Ar flux with a suitable controller (LINKAM - LNP) connected to the stage of the probing system. The temperature was measured by thermocouples within the stage. The heating rate was of 10 °C/min and the resistivity measurements were performed every 30 °C during the initial part of the heating (i.e. until ~300 °C), then steps were decreased to down to 10 °C once the expected T_g was approached, to better characterize the structural evolution of the samples. For each step, the system was subjected to isothermal conditions for 3 min. One minute of waiting time was necessary to reach the thermal equilibrium, and then data were acquired during the remaining 2 min. A total of 100 direct

current pulses of 50 mA have been applied by a Keithley 6221 function generator with a pulse width of $5 \cdot 10^{-3}$ s, while the voltage was measured at the pulse half-time through a Keithley 2182A nanovoltmeter. The resistivity is averaged over 100 measurements per temperature step.

2.5 Mechanical characterization

2.5.1 Optoacoustic techniques

Brillouin light scattering (BLS) and picosecond laser ultrasonic (PLU) experiments were carried out to extract the elastic constants. BLS spectra were acquired in air at room temperature with an incidence angle of 65°, with acquisition times of 1 h and 200 mW of a p-polarized incident light (λ = 532 nm). The technique allows the extraction of the Rayleigh surface wave sound velocity (V_R) which can be directly connected to the shear sound velocity (V_S) and shear modulus $G = C_{44} = \rho(V_S)^2$ by knowing the mass density (ρ). Further details are available in Ref. [31] and the Supplementary Information for the extraction of the elastic constants. For the PLU experiment, an ultrashort light pulse is focused on the film, generating an elastic strain pulse consisting mainly of longitudinal acoustic phonons that propagate as coherent waves. The waves are then reflected at the interface between film and substrate and the time of flight (*TOF)* of the wave is thus measured by observing the relative variation of the probe reflectivity when the echoes reach the free surface. By knowing the thickness (*t)* of the film, it is possible to obtain the longitudinal velocity V_L with the relationship $V_L = 2t/TOF$, which can be connected with elastic properties.

2.5.2 Nanoindentation

Nanoindentation experiments were performed with a KLA G200 nanoindenter, equipped with a DCM head and a diamond Berkovich tip (Synton-MDP, Switzerland). The measurements were carried out using the continuous stiffness measurement (CSM) method [32], to measure both elastic modulus (*E*) and hardness (*H*) as a function of indentation depth. A standard fused silica sample was used before and after the measurements for tip and frame stiffness calibrations. A minimum of 25 indentations were performed on each sample, *E* and *H* have been extracted at indentation depths ~10% of the film thickness [33]. The strain rate sensitivity (*m*) of the hardness was calculated using $\partial lnH/\partial ln\dot{\varepsilon}$ where $\dot{\varepsilon}$ is the representative

indentation strain rate [34]. This strain rate $\dot{\varepsilon}$ can be estimated as $\dot{P}/2P$ where $\dot{P}/P$ is the (constant) loading rate. Three different constant loading rates equal to 0.02, 0.05 and 0.1 s^{-1} were used. The activation volume (V_a) is equal to $3\sqrt{3}kT/mH$ where *k* is the Boltzmann constant, *T* is the test temperature and *H* is the mean hardness over the range of strain rates [34, 35].

2.5.3 Tensile tests on polymeric substrates

Tensile tests were performed on films deposited on 120 μm thick flexible Kapton® substrates, using a 300 N Deben tensile machine combined with a Keyence confocal microscope [36]. The tensile speed was 0.5 mm/min and the initial sample length was of 40 mm, corresponding to a strain rate of ~2.1×10^{-4} s^{-1}. A 10x objective was used for monitoring the crack density evolution as a function of the applied strain. The linear crack density was calculated by measuring the number of cracks (orthogonal to the loading direction) over the length of the sample captured by the microscope objective (i.e. 1050 μm).

2.6 *Ab initio* molecular dynamics and atomic cluster analysis

AIMD have been used to simulate the amorphous structure with the aim to analyze the local order as a function of the Al content, relating the atomic arrangement to the mechanical properties and thermal stability. First-principles calculations were performed with the Vienna Ab initio Simulation Package (VASP) [37]. 256 atoms of $ZrCuAl_x$ (x = 0, 6, 9, 12 at.%) were placed in a cubic box with periodic boundary conditions. All the alloys were first melted at 2500 K and maintained at this temperature for at least 11 ps using the isobaric-isothermal (NPT) ensemble to obtain a homogeneous molten alloy. The system was then continuously quenched from 2500 down to 300 K at a cooling rate of 733×10^{13} K/s (0.3×10^{-15} s time step and 1000 steps) and then relaxed at 300 K. Elastic constants C_{ij} were then investigated at 0 K by employing the stress-strain method ($\sigma = C\varepsilon$) [38], considering the possibility for atoms positions to be relaxed or not relaxed after each strain. The last thousand time steps of quenched alloys were analyzed by the Voronoi tessellation method using the OVITO software package [39]. In the Voronoi tessellation analysis, the five indices < n_3 n_4 n_5 n_6 n_7 >, are attributed to each polyhedral cell, where n_i is the number of faces with *i*-edges

in each Voronoi cell (i.e. the icosahedra named with a Voronoi index of < 0 0 12 0 0 >) and Σn_i is the coordination number [40].

3. Results

3.1 Structural characterization

Fig. 2 (a-d) shows the SEM cross-sectional view of the $ZrCuAl_x$ TFMGs with Al content from 0 up to 12 at.%. The surface of fracture was observed after cracking the Si wafers using cleaving pliers from a narrow notch induced by a diamond tip. The thickness measured by cross section SEM imaging is equal to 800 ± 20 nm for all the specimens, in particular it resulted around 780 nm for $Zr_{50}Cu_{50}$ and 820 nm for all the ZrCuAl films. The presence of corrugations on the fracture surface is a consistent feature of metallic glasses [11, 41]. These corrugations are specifically related to shear band propagation by nanometric mechanisms linked to atomic cavitation, and the toughness of the material can be directly correlated with their size [41]. The ZrCu and $ZrCuAl_x$ TFMGs presented an average length (thickness direction) of the corrugations of 80 ± 20 nm and a width of 50 ± 15 nm which are in agreement with other works on Zr-based TFMGs [41, 42]. It is worth to notice that the discrepancy in film thickness observed in **Fig. 2a** might be related to the slanted fracture surface of the film towards Si substrate, affecting the thickness measurements.

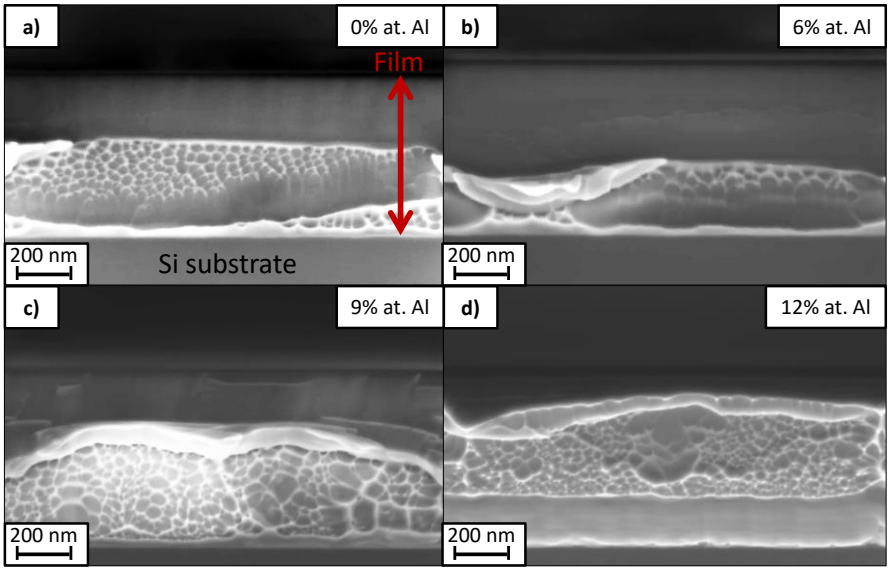

Fig. 2: (a-d) SEM cross-sectional images of $ZrCuAl_x$ with different Al content from 0 to 12 at.%. Corrugations are visible on all fracture surfaces.

The pair distribution functions (PDFs) of $ZrCuAl_x$ TFMGs extracted from sXRD measurements are presented in **Fig. 3**. The position of first peak represents the average interatomic distances between atoms within the first coordination shell. $Zr_{50}Cu_{50}$ revealed an average interatomic distance of 2.6 Å, in good agreement with what was found by Mattern *et al*. [43] which measured experimentally the PDF of bulk $Zr_{50}Cu_{50}$ by X-ray and neutron diffraction, reporting an average atomic distance of 2.7 Å. The Al addition induces a slightly shift of the first peak towards lower atomic distances down to 2.5 Å for all the compositions of $ZrCuAl_x$ (inset in **Fig. 3**). The shortening in average interatomic distances is due to several factors such as the formation of shorter Zr-Al [25] and Cu-Al [44, 45] bonds and the stress field in the material. For instance, Yang *et al.* [25] demonstrated by sXRD and EXAFS measurements on bulk $Zr_{48}Cu_{45}Al_7$ that after annealing, the relaxation process can affect the position of the first peak of partial PDFs for Zr-Al bonds which shift towards larger distances (from 2.5 to 2.7 Å) changing the short-range order. Finally, the presence of two superposed peaks within the second band of the PDF is observed between 4 and 6 Å. This feature is a typical fingerprint of metallic glasses which reflect a medium range order [46].

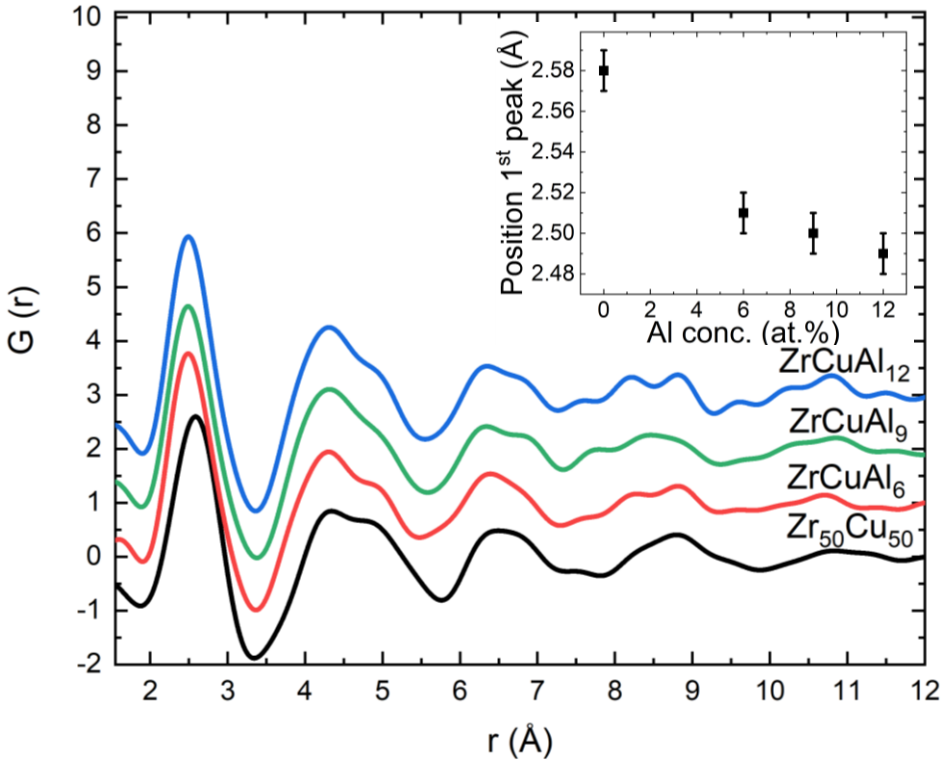

Fig. 3: Pair distribution function G(r) of $ZrCuAl_x$ TFMGs at T_{room}. The inset shows the mean position (± 1 pm) of the first peak as a function of the Al content.

3.2 Thermal stability

XRD analysis at T_{room} showed the presence of two broad diffraction humps located at ~37-38° and 68-69° confirming the amorphous structure of $ZrCuAl_x$ films (**Fig. 4**). The position and full width at half maximum (FWHM, ~7.5°) are not influenced by the Al addition due to its small content and the values are coherent with what has been reported in literature [18, 47]. Moreover, the average atomic distance *d*, obtained through the Ehrenfest equation [48] applied on the first peak amounts in all measurements to 290 ± 10 pm. This value agrees with the synchrotron measurements which show a weak trend in the variation of atomic distances with Al content (**Fig. 3**). However, the XRD data does not reveal any shift of the average interatomic distance because of the low energies involved and the lower Q-resolved diffractogram compared to synchrotron-source experiment.

The thermal stability of the $ZrCuAl_x$ TFMGs have been investigated by performing XRD measurements as a function of the temperature (up to 600°C), aiming also to obtain the crystallization temperature (T_x). **Fig. 4** reports oxidation phenomena with the formation of crystalline ZrO_2 and Al_2O_3 followed by crystallization phase with the formation of ZrCuAl intermetallic compounds occurring for all the investigated $ZrCuAl_x$ compositions. The presence of oxides is likely due to residual O during XRD measurement, which reacts preferentially with Zr and Al due to their high O affinity [49, 50]. As an example, in the case of $ZrCuAl_6$ (**Fig. 4a**), the amorphous state is confirmed by the presence of the two typical humps at 38 and 68° at T_{room} up to 390 °C. Then, the formation of first oxidation phases are observed at 420 °C and are related to the formation of ZrO_2 and Al_2O_3 identified from the sharp peaks at 35, 50, 60°. Finally, when the temperature reaches 450 °C, crystallization occurs with the formation of cubic $Zr_6Cu_{16}Al_7$ and cubic ZrCuAl (peaks at 43, 46, 50°). The formation of other intermetallic compounds (such as Al_2Zr and $ZrCu_{0.5}Al_{2.5}$) at 540 °C suggests further phase transformations after crystallization. A detailed phase analysis of $ZrCuAl_6$ TFMG at 600°C is reported in the Supplementary Information (**Table S1** and **Fig. S1**).

From the comparison of different Al contents in **Fig. 4**, the oxidation temperature increases with Al addition and reaches 480 °C for 12 at.% Al. A similar trend is detected for T_x which increases from 390 °C for

$Zr_{50}Cu_{50}$ up to 510 °C for $ZrCuAl_{12}$in which complete crystallization occurs, highlighting the stabilizing effect of Al on the amorphous structure which is in good agreement with the literature [18, 51].

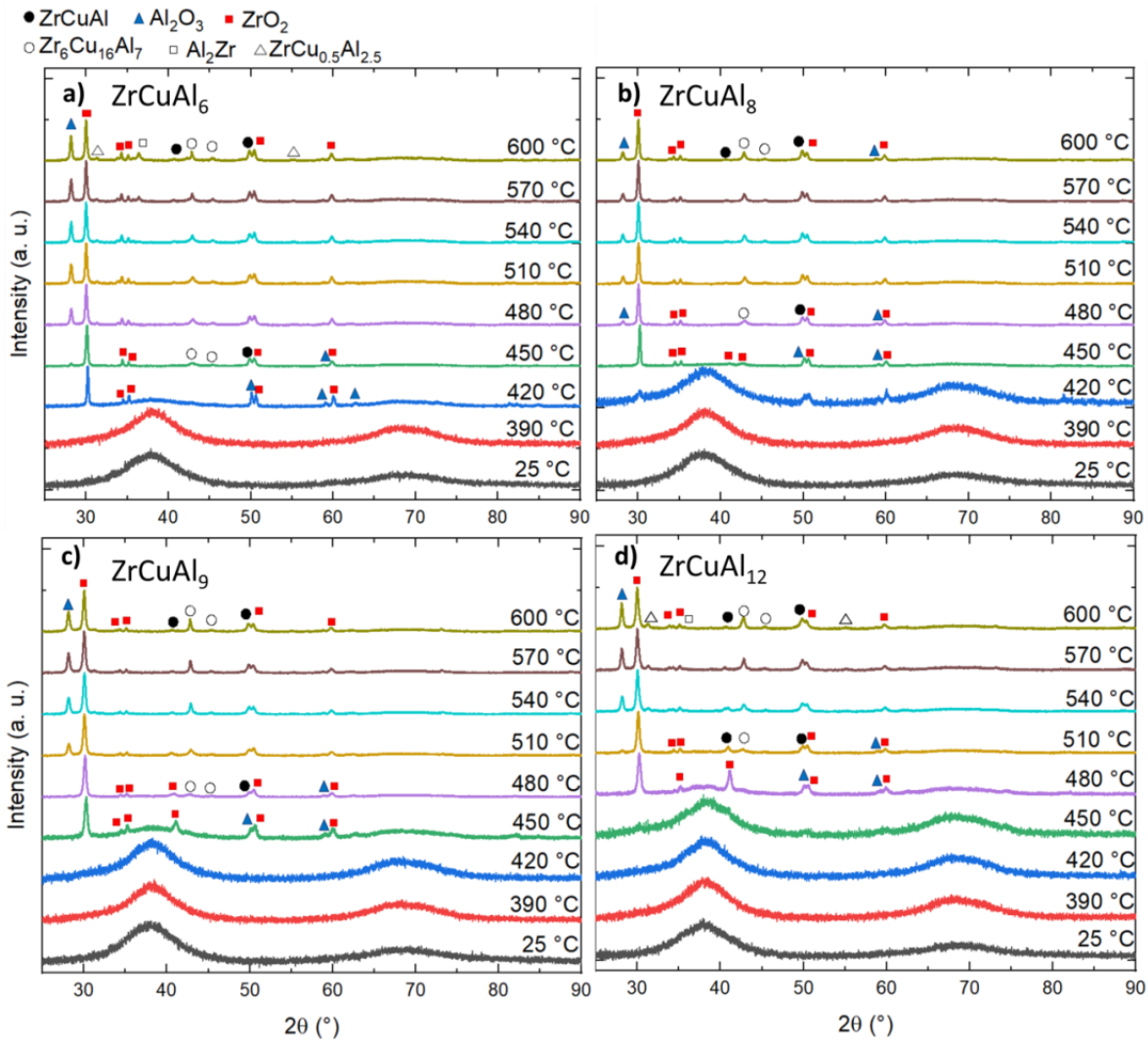

Fig. 4: XRD diffractograms as function of temperature for different $ZrCuAl_x$ TFMGs. Note the increase in crystallization temperature with increasing Al content.

To get a comprehensive understating of the evolution on the atomic structure during crystallization and of the effect of oxidation, *in situ* XRD heating measurements were performed under high vacuum conditions using a synchrotron source. The diffractograms series are reported in Supplementary Information (**Fig. S2**) and an example is reported for $ZrCuAl_{12}$ in **Fig. 5**. At T_{room}, the structure factor *S(Q)* shows two broad peaks centered at 3.12 and 5.17 $Å^{-1}$, typical of an amorphous structure. During heating, all the $ZrCuAl_x$ TFMGs showed a similar behavior with a shift of the first peak towards higher *Q* (from 3.12 to 3.14 $Å^{-1}$), while the

second broad peak shifts in the opposite direction (from 5.17 to 5.12 $Å^{-1}$) indicating a change in atomic configuration before crystallization due to relaxation phenomena [52, 53]. ZrCu films showed an analogous behavior, in which the two peaks shift from 3.04 to 3.06 $Å^{-1}$ and 5.11 to 5.05 $Å^{-1}$, respectively. From temperatures higher than 500 °C a clear transition from an amorphous to crystalline structure occurs, evidenced by the increase in intensities of the first and second humps followed by the presence of sharp diffraction peaks over the Q-space indicative of long-range ordering. All the $ZrCuAl_x$ presented the same crystallization behavior and a detailed phase analysis of $ZrCuAl_{12}$ is reported in **Fig. S3**. Cubic $CuZr_2$, tetragonal $CuZr_2$ and cubic ZrCu phases are formed during the crystallization. The formation of tetragonal $CuZr_2$ has been observed in other works in annealed ZrCu [11, 54] and in particular Liu *et al.* showed by synchrotron diffraction that during annealing tetragonal $CuZr_2$ transforms into cubic $CuZr_2$ in ZrCuAl alloys [55]. Furthermore, the same cubic $Al_{2.5}Cu_{0.5}Zr$ phase was observed as for XRD, while there was no evidence of oxides since experiments are carried out in high vacuum.

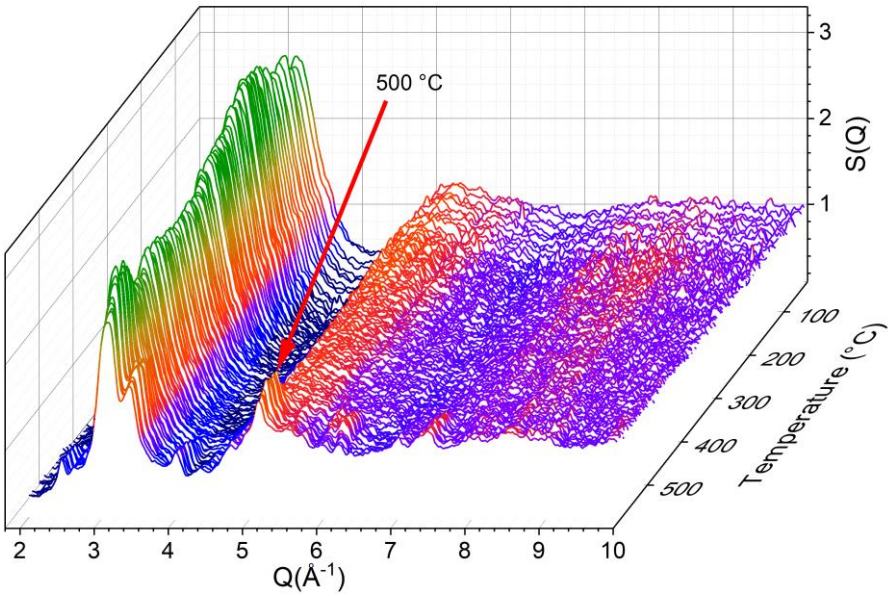

Fig. 5: Evolution of structure factor *S(Q)* of $ZrCuAl_{12}$ as function of temperature.

The thermal stability of $ZrCuAl_x$ TFMGs was further investigated by analyzing the electrical resistivity (ρ_E) as function of the temperature, enabling a more precise estimation of the glass transition temperature (T_g). For more details, the reduced electrical resistivity measurements (ρ_E/ρ_0) as function of the temperature are

represented in the Supplementary Information in **Fig. S4** which include the procedure of extrapolation of characteristic temperatures (T_g and T_x) as for Ref. [56]. For all the samples, the measured values of electrical resistivity (~170 μΩ cm) did not show any detectable variation as a function of Al content while being in agreement with the literature of amorphous Zr-based metallic glasses [57, 58].

Overall, the T_x of ZrCuAl TFMGs, as well as T_g from resistivity measurements, increases with the Al content confirming the increase of thermal stability of the amorphous phase, as has been observed in literature data for $ZrCuAl_x$ TFMGs [28, 59]. A good agreement for T_x values found by the different techniques was observed. However, a difference in T_x (between 20 and 30 °C) was observed for $ZrCuAl_6$ TFMGs (**Fig. 6**). This might be related to the small differences in thermal histories (heating rates and isothermal segments) described in **Sections 2.3 and 2.4** or to the oxidation during XRD measurements. Oxides, as inhomogeneities, could act as "nucleation sites" catalyzing the transition and influencing the crystallization temperature. Of note, Zhang *et al.* [60] showed that ZrO_2 nanocrystals nucleated in $Zr_{55}Cu_{30}Al_{10}Ni_5$ amorphous film act as nucleation cores and diffusion paths for oxygen. Moreover, the formation of Al and Zr oxides enriches the glassy matrix of Cu atoms, changing the composition and leading to a less thermal stable alloy [61]. Finally, the physical reason for the increasing thermal stability for large Al content is related with the formation of shorter Zr-Al bonds which reduces the atomic mobility of large Zr-centered and Cu-centered clusters. Moreover, Al atoms can act like "pins", limiting the arrangement of clusters during crystallization and stabilizing the local structure [25, 45].

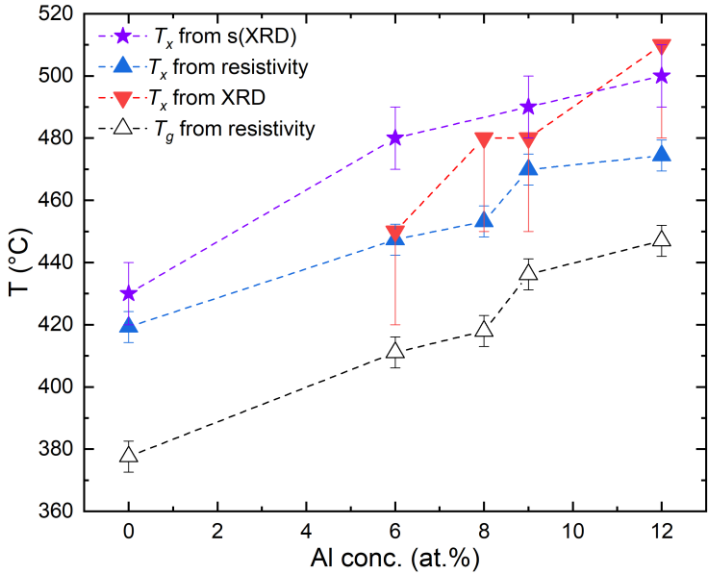

Fig. 6: Comparison of characteristic temperatures T_g (empty symbols) and T_x (filled symbols) of $ZrCuAl_x$ TFMGs obtained with different techniques.

3.3 Mechanical characterization

The elastic constants and moduli were measured by nanoindentation and optoacoustic techniques, and predicted by first-principles calculations. **Fig. 7a** shows the shear modulus *G* measured by BLS and Poisson's ratio (see Supplementary Information Section 4 for more details and Ref. [35]). The shear modulus monotonically increases from 30 to 35 GPa and similar values (between 32 and 36 GPa) are found in literature for bulk ZrCuAl metallic glasses [17]. The Poisson's ratio values remained constant and equal to ~0.37 for Al content up to 9 at.%, while decreasing to ~0.35 with further Al addition , indicative of a lower fracture toughness [62]. A similar transition in Poisson's ratio was observed by Yu *et al.* [17]. The authors measured, by ultrasound techniques in the MHz regime, a maximum of Poisson ratio of 0.37 for bulk $Zr_{47.5}Cu_{47.5}Al_5$, which monotonically decreased by further addition of Al to 0.36 for $Zr_{45}Cu_{45}Al_{10}$. **Fig. 7b** shows that the hardness increases monotonically from 6.8 to 7.8 GPa and the Young' modulus measured by nanoindentation and optoacoustic techniques increases from 100 and 85 up to 115 GPa and 95 GPa, respectively, for 0 and 12 at.% Al. The difference in the elastic modulus measured by nanoindentation and optoacoustic is ~15%, in agreement with other works [11, 63]. The stiffening of the material by increasing the Al content is in good

agreement with what has been observed for BMGs and is mainly related to the formation of shorter and stronger Zr-Al and Cu-Al bonds as confirmed from the shift towards lower values of the average interatomic distances in sXRD measurements [29].

The elastic constants and moduli were also predicted by density functional theory (DFT) calculations at 0 K referring to both relaxed and unrelaxed structure (where atoms are allowed or not to relax after straining the cell, respectively). In **Fig. 7a-b**, the simulated elastic moduli (*G* and *E*) and ν values show the same trend of those measured experimentally (increasing about ~15% by increasing the Al content) which fall in the average of relaxed and unrelaxed structures.

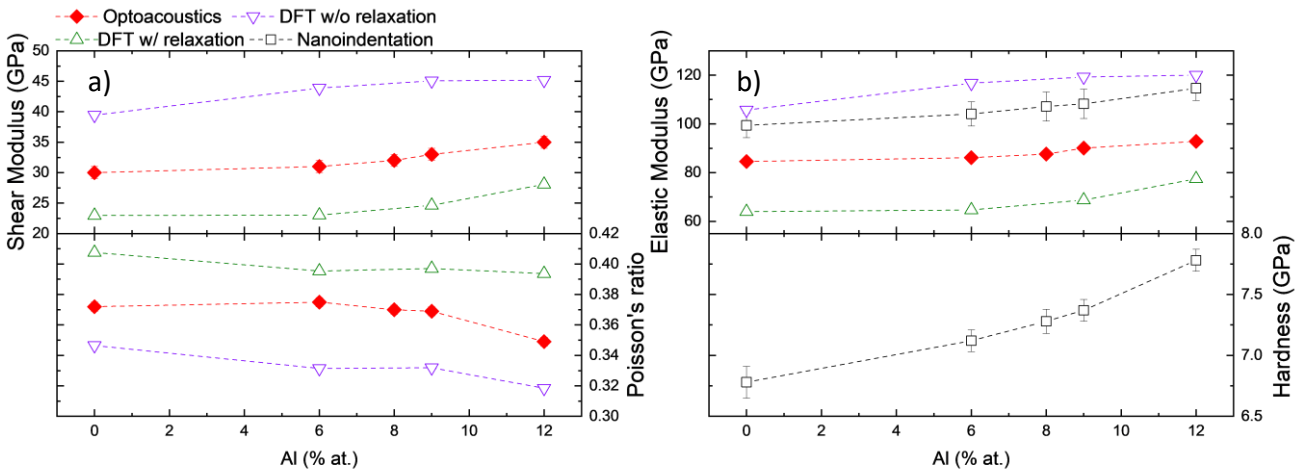

Fig. 7: (a) Evolution of shear modulus and Poisson's ratio and (b) Young's modulus and hardness of ZrCuAl as a function of the Al content. The dotted lines in the figures are for visualization purposes only.

The investigation of strain rate sensitivity was performed by nanoindentation with three different loading rates (i.e. 0.02, 0.05 and 0.1 s^{-1}). The interval in which *E* and *H* were extracted and the load curves are reported in **Fig. S6**. The hardness of all the investigated samples increases by increasing the strain rate due to the viscoelastic behavior of metallic glass [64]. For example, *H* of $ZrCuAl_8$ increases from 7.0 up to 7.3 GPa while increasing the strain rates from 0.01 up to 0.05 s^{-1}. The slope of the linear fit of *H* defines the strain rate sensitivity (*m*) shown in **Fig. 8b** which decreases slightly from 0.026 down to 0.023 ± 1.5 × 10^{-3} at 9 at.% Al and it further decreases to 0.019 ± 1.5 × 10^{-3} for $ZrCuAl_{12}$. The values of *m* are coherent with what was found in 900 nm-thick ZrCuAl TFMGs by Ma *et al.* [65] and Sun *et al.* [66], but they are about two times higher than

those found for BMGs [18], suggesting an intrinsic difference between atomic structure of bulk and thin films materials due to the different synthesis methods, resulting in changes in local order and free volume content. The corresponding activation volume was nearly constant and ranged from 119 ± 7 for $Zr_{50}Cu_{50}$ up to 139 ± 7 $Å^3$ for 12 at.% Al. Das *et al*. [19] reported that the Al addition causes the formation of structural inhomogeneities in the material favoring the nucleation of multiple shear bands. This would be coherent with the measured increase in activation volume. Specifically, Pan *et al.* [34] observed that a large size of shear transformation zones (which are directly proportional with activation volume) promotes the formation of multiple shear bands which intersect each other, hindering the propagation and leading to global ductility of the material.

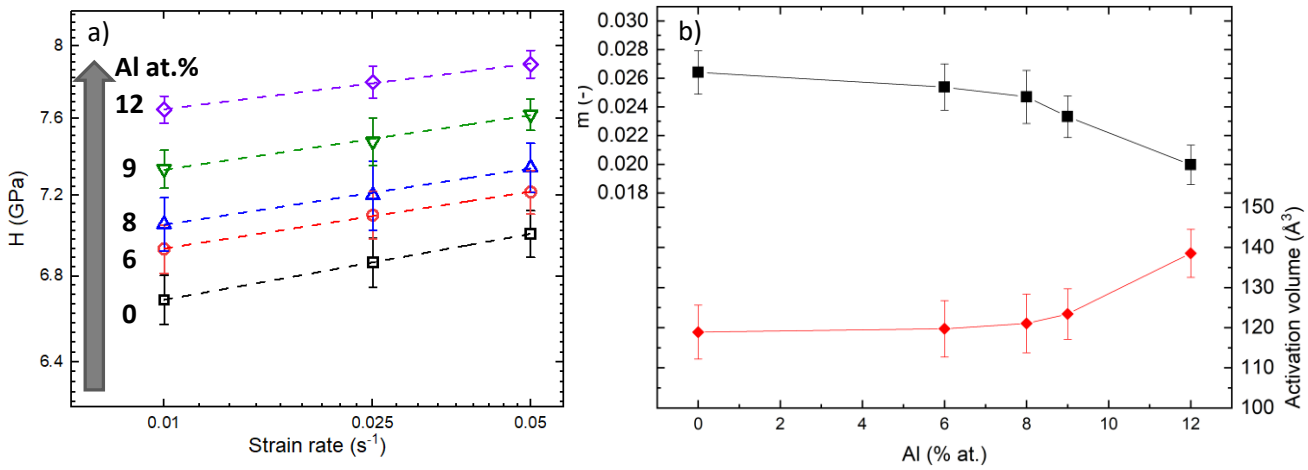

Fig. 8: Evolution (a) of hardness as a function of the strain rate for different Al contents and (b) evolution of the strain rate sensitivity and activation volume as a function of Al % at.

The mechanical response of $ZrCuAl_x$ TFMGs was further evaluated by analyzing the cracking behavior during tensile testing on polymeric (Kapton®) substrates. **Fig. 9a** represents the evolution of crack density as function of the applied strain. As first information, the onset of crack formation increases from ~1 up to ~2.1% by increasing the Al content up to 9 at.%, while for further additions of Al (i.e. 12 at.%) an embrittlement is observed with a lower onset of crack formation ~0.8% and the highest saturation crack density (**Fig. 9b**). This is related to a lower toughness of the material (lower Poisson's ratio) [36, 67], while other effects including the adhesion with the interface with polymeric substrate can also be affected. As soon as the first crack

appears, its morphology gives some insights to the ductile/brittle behavior of $ZrCuAl_x$ thin films. The top view images by confocal microscope are represented as function of the applied deformation in **Fig. S7.** Ductile features, such as crack-blocking phenomena and crack deviations were observed for TFMGs with Al content equal to 9 at.% (inset in **Fig. 9a**), while for $ZrCuAl_{12}$ the cracks are straight and propagate through the whole length of the sample which is a characteristic feature of brittle films [36].

Brognara *et al.* [11] analyzed the cracking behavior of three different composition of 400 nm-thick $Zr_{100-x}Cu_x$ TFMGs by tensile tests on Kapton® finding a crack initiation strain between 0.5 and 2% which are coherent with values of this work. However, the presence of a nanocolumnar structure in their work for $Zr_{52}Cu_{48}$ film lead to a lower crack initiation strain ~0.5% that is two times less than the value measured for compact $Zr_{50}Cu_{50}$ investigated in this work. Nevertheless, the authors also stated that the interfaces between the nanocolumns of $Zr_{52}Cu_{48}$ could act as preferential crack initiation sites lowering the resistance of the film. Furthermore, a maximum in crack initiation strain (~2.1%) was found for $Zr_{24}Cu_{76}$ and this was justified with the larger volume fraction of full icosahedral atomic packing present in Cu-rich ZrCu films, which is known to improve the resistance of the system to shear instabilities [68].

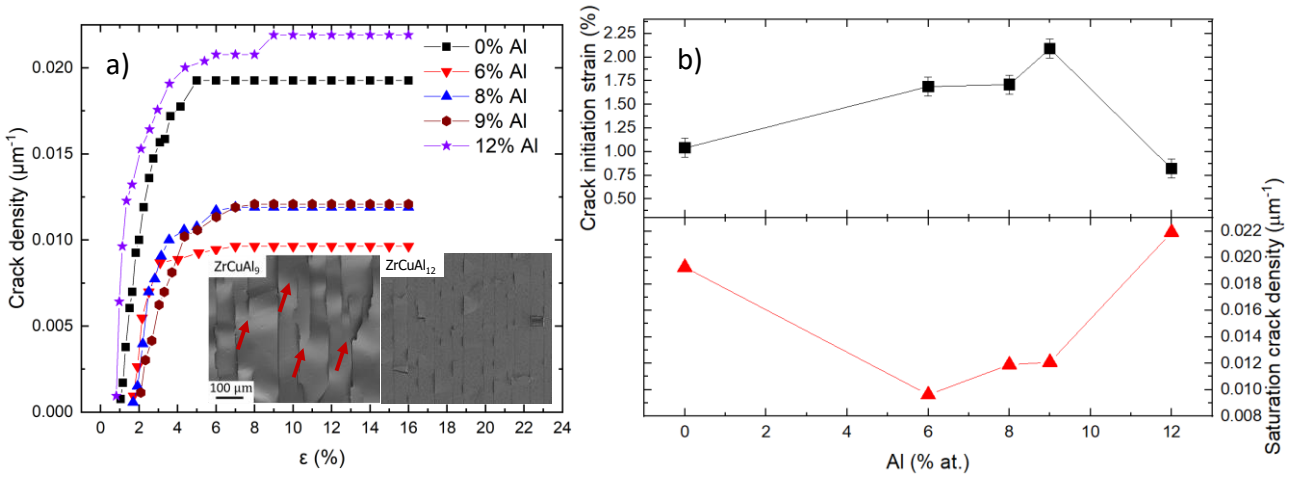

Fig. 9: Evolution of the (a) crack density, (b) crack initiation strain and saturation crack density of ZrCuAl as a function of Al content. The inset for (a) shows the *post mortem* SEM image of the top view of $ZrCuAl_9$ (left) and $ZrCuAl_{12}$ (right) TFMG. The red arrows indicate crack stopping and deflecting phenomena occurring in $ZrCuAl_9$.

4. Discussion supported by *ab initio* calculations

For a comprehensive understanding of the structure, thermal stability and mechanical behavior, we carried out an analysis of the topological short-range order by Voronoi tessellation quantifying the fraction of full and defective icosahedral population [40]. Jawaid *et al.* [69] analyzed the Voronoi polyhedral population for different compositions of ZrCu and showed the maximum of glass forming ability (and thus of the thermal stability) for $Zr_{40}Cu_{60}$, reporting a maximum in Cu-centered icosahedra < 0 0 12 0 0 >. The presence of full-icosahedra maximizes the packing efficiency of atoms and provides a more ordered structure, increasing the density of the material and reducing the free volume content. The larger atomic volume of Zr-centered polyhedral population does not influence the thermal stability because they reduce the density of the system as reported in Ref. [70]. Therefore, the thermal stability and thermal behavior is dictated mainly by the population of Cu- and Al-centered clusters [70]. **Fig. 10** shows that the Al addition strongly affects the population of Cu-centered full icosahedra (< 0 0 12 0 0 >) from 2 to 8% resulting in the progressively higher thermal stability and stronger mechanical behavior. This is in agreement with synchrotron experiments showing that Al provides shorter and stronger chemical bonds reducing the atomic mobility and inhibiting the crystallization behavior [25, 45]. This has been also related to an increase of elastic moduli (*E* and *G*) and hardness reaching a maximum of respectively 115, 36 and 7.8 GPa. However, the activation volume was nearly constant (~ 130 $Å^3$), suggesting there are not significant changes in the shear transformation zone volumes for plastic flow. The total fraction of population of Cu-centered full and defective icosahedra < 0 2 8 1 0 >, < 0 2 8 2 0 > and < 0 1 10 2 0 > shows a maximum for 9 at.% Al and a similar trend was observed for the full and defective Al-centered polyhedral population. This has been related to the large shear-resistance behavior [68], with the largest onset of crack formation on polymeric substrate up to 2.1%. This trend has been reported also by Abbasi *et al.* [70] demonstrated by MD simulations. For Al contents larger than 9 at.%, the fraction of full and defective Al-centered icosahedra decreases, suggesting the formation of new different polyhedral configurations in which the excess of Al atoms bonds with existing Cu-centered icosahedra,

causing their distortion and a change in the local order which in turn result in a pure mechanical behavior (onset crack initiation strain of ~0.7%).

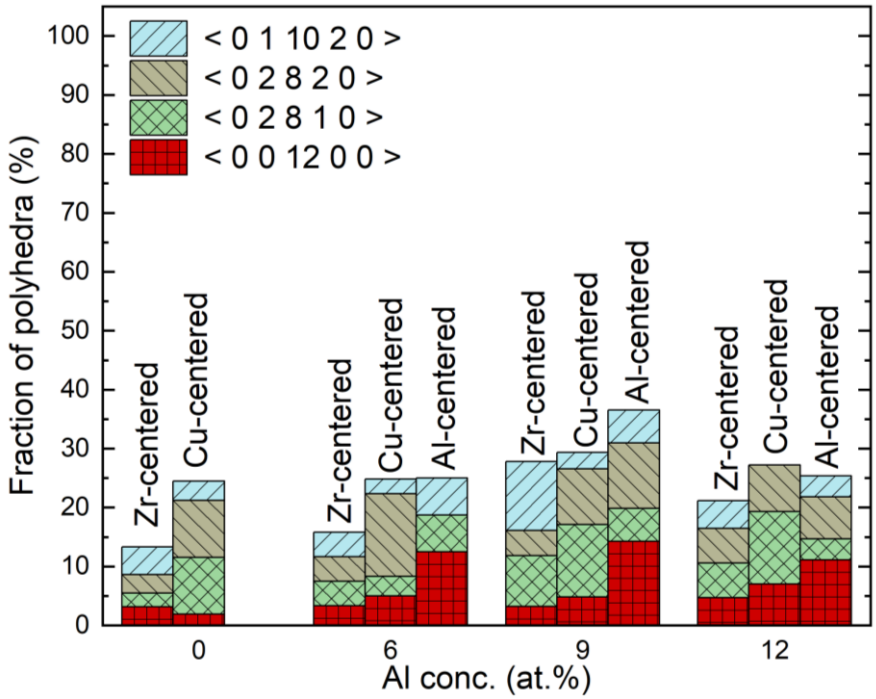

Fig. 10: Full and defective Zr, Cu and Al-centered polyhedral population calculated for $ZrCuAl_x$ (x = 0, 6, 9, 12 at.%).

Conclusions

In this work $ZrCuAl_x$ TFMGs with Al content x = 0-12 at.% were deposited by magnetron sputtering and characterized to understand the effect of composition on the atomic structure, mechanical properties and thermal stability. It was found that:

- The average interatomic distances of $Zr_{50}Cu_{50}$ is ~2.6 Å and the addition of Al promoted the formation of shorter bonds (Zr-Al and Al-Cu) reducing the average interatomic distances down to 2.5 Å without any further shift upon addition of Al. The activation volume (calculated by nanoindentation at different strain rates) is almost constant (from 120 ± 7 for $Zr_{50}Cu_{50}$ up to 139 ± 7 $Å^3$ for 12 at.% Al) indicating similar deformation mechanisms involved in the formation of shear band instabilities.
- The addition of Al increases the thermal stability of the films, increasing T_g and T_x from 380 and 430 (0 at.% Al), up to 440 °C and 500 °C for $ZrCuAl_{12}$. This is related to the full Cu-centered icosahedral

population and to the reduced atomic mobility of the Zr and Cu clusters due to the formation of short and strong Al bonds.

- The evolution of the elastic properties (*G*, *E*) and hardness (*H*) shows a monotonic increase of ~10% from 30 GPa, 83 GPa and 6.7 GPa, respectively, for ZrCu to 35 GPa, 95 GPa and 7.8 GPa for $ZrCuAl_{12}$. This has been related with the increase of the number of Al-centered polyhedra providing stiffer atomic bonds and larger stability against shear band propagation.
- The tensile tests of TFMGs deposited in polymeric substrates show that the resistance to crack initiation improves with the addition of Al up to 9 at.% and then abruptly decreases, in agreement with the small decrement in Poisson's ratio, reducing the toughness. Furthermore, the Voronoi tessellation analysis of $ZrCuAl_9$ revealed a peculiar cluster coordination composed with the highest fraction of full and defective icosahedra responsible of the large shear-resistant behavior.

In conclusion, in this work we provide a complete picture about the relationship between atomic structure, mechanical properties and thermal stability for $ZrCuAl_x$ TFMGs. Specifically, the addition of small quantities of Al influences the atomic configuration and the local chemical order promoting both thermal stability and overall mechanical properties of ZrCuAl TFMGs reaching optimal values for 9 at.% Al. Overall, these results provide guidelines to the design of compositional-tailored $ZrCuAl_x$ TFMGs with potential impact on industrial applications as structural coatings with large mechanical properties and high thermal stability, preventing devitrification phenomena.

Acknowledgements

M. Ghidelli and C. Poltronieri acknowledge the financial support of Partenariats Hubert Curien (PHC) PROCOPE 2021 project ''New-Glasses" (Grant #46735ZG) financing the cooperation between Max-Planck Institut für Eisenforschung GmbH (MPIE) and Laboratoire des Sciences des Procédés et des Matériaux (LSPM). J.P. Best and A. Brognara acknowledge the Deutsche Akademische Austauschdienst (DAAD) within program "Programme des projektbezogenen Personenaustauschs (PPP)" (Project-ID: 57561649) financed by the Bundesministerium für Bildung und Forschung (BMBF). F. Bignoli acknowledges the financial support of the

Université Franco Italienne (UFI) for the funding of his PhD scholarship through a Vinci Cap. III Grant (#C3-2286). We acknowledge DESY (Hamburg, Germany), a member of the Helmholtz Association HGF, for the provision of experimental facilities. Parts of this research were carried out at PETRA III at the P21.1 beamline through proposal I-20211503, and the authors acknowledge Ida Gjerlevsen Nielsen, Ann-Christin Dippel, Olof Gutowski, and Philipp Glaevecke for their support.

Declaration of competing interest

The authors declare that they have no known competing financial interests or personal relationships that could have appeared to influence the work reported in this paper.

References

[1] M. Ashby, A. Greer, Metallic glasses as structural materials, Scr. Mater. 54(3) (2006) 321-326.
[2] C.A. Schuh, T.C. Hufnagel, U. Ramamurty, Mechanical behavior of amorphous alloys, Acta Mater. 55 (2007) 4067-4109.
[3] A.L. Greer, Y.Q. Cheng, E. Ma, Shear bands in metallic glasses, Mater. Sci. Eng., R 74(4) (2013) 71-132.
[4] J.P. Chu, J.S.C. Jang, J.C. Huang, H.S. Chou, Y. Yang, J.C. Ye, Y.C. Wang, J.W. Lee, F.X. Liu, P.K. Liaw, Y.C. Chen, C.M. Lee, C.L. Li, C. Rullyani, Thin film metallic glasses: Unique properties and potential applications, Thin Solid Films 520(16) (2012) 5097-5122.
[5] M. Ghidelli, H. Idrissi, S. Gravier, J.-J. Blandin, J.-P. Raskin, D. Schryvers, T. Pardoen, Homogeneous flow and size dependent mechanical behavior in highly ductile Zr65Ni35 metallic glass films, Acta Materialia 131 (2017) 246-259.
[6] L. Tian, Y.Q. Cheng, Z.W. Shan, J. Li, C.C. Wang, X.D. Han, J. Sun, E. Ma, Approaching the ideal elastic limit of metallic glasses, Nat. Commun. 3:609 (2012) 1-6.
[7] M. Ghidelli, A. Orekhov, A.L. Bassi, G. Terraneo, P. Djemia, G. Abadias, M. Nord, A. Béché, N. Gauquelin, J. Verbeeck, J.P. Raskin, D. Schryvers, T. Pardoen, H. Idrissi, Novel class of nanostructured metallic glass films with superior and tunable mechanical properties, Acta Materialia 213 (2021) 116955.
[8] L. Tian, Z.-W. Shan, E. Ma, Ductile necking behavior of nanoscale metallic glasses under uniaxial tension at room temperature, Acta Mater. 61(13) (2013) 4823-4830.
[9] Q. Deng, Y. Cheng, Y. Yue, L. Zhang, Z. Zhang, X. Han, E. Ma, Uniform tensile elongation in framed submicron metallic glass specimen in the limit of suppressed shear banding, Acta Mater. 59(17) (2011) 6511-6518.
[10] H. Guo, P.F. Yan, Y.B. Wang, J. Tan, Z.F. Zhang, M.L. Sui, E. Ma, Tensile ductility and necking of metallic glass, Nature Mater. 6(10) (2007) 735-9.
[11] A. Brognara, J.P. Best, P. Djemia, D. Faurie, G. Dehm, M. Ghidelli, Effect of composition and nanostructure on the mechanical properties and thermal stability of Zr100-xCux thin film metallic glasses, Materials & Design 219 (2022) 110752.

[12] F. Bignoli, S. Rashid, E. Rossi, S. Jaddi, P. Djemia, G. Terraneo, A. Li Bassi, H. Idrissi, T. Pardoen, M. Sebastiani, M. Ghidelli, Effect of annealing on mechanical properties and thermal stability of ZrCu/O nanocomposite amorphous films synthetized by pulsed laser deposition, Materials & Design 221 (2022).
[13] S. Lee, S.W. Kim, M. Ghidelli, H.S. An, J. Jang, A.L. Bassi, S.Y. Lee, J.U. Park, Integration of Transparent Supercapacitors and Electrodes Using Nanostructured Metallic Glass Films for Wirelessly Rechargeable, Skin Heat Patches, Nano letters 20(7) (2020) 4872-4881.
[14] S. Evertz, V. Schnabel, M. Köhler, I. Kirchlechner, P. Kontis, Y.-T. Chen, R. Soler, B.N. Jaya, C. Kirchlechner, D. Music, B. Gault, J.M. Schneider, D. Raabe, G. Dehm, Review on Quantum Mechanically Guided Design of Ultra-Strong Metallic Glasses, Frontiers in Materials 7 (2020).
[15] J.J. Lewandowski, W.H. Wang, A.L. Greer, Intrinsic plasticity or brittleness of metallic glasses, Philosophical Magazine Letters 85(2) (2005) 77-87.
[16] K. Liang, X. Zhang, J. Qiao, S. Pan, S. Feng, Effects of minor addition of Al and Ag elements on the atomic structure and mechanical property of ZrCu-based metallic glasses, Journal of Non-Crystalline Solids 550 (2020) 120385.
[17] P. Yu, H.Y. Bai, Poisson's ratio and plasticity in CuZrAl bulk metallic glasses, Materials Science and Engineering: A 485(1-2) (2008) 1-4.
[18] R. Limbach, K. Kosiba, S. Pauly, U. Kühn, L. Wondraczek, Serrated flow of CuZr-based bulk metallic glasses probed by nanoindentation: Role of the activation barrier, size and distribution of shear transformation zones, J. Non-Cryst. Solids 459 (2017) 130-141.
[19] J. Das, M.B. Tang, K.B. Kim, R. Theissmann, F. Baier, W.H. Wang, J. Eckert, "Work-Hardenable" ductile bulk metallic glass, Physical review letters 94(20) (2005) 205501.
[20] Y. Chen, J.-Z. Jiang, Formation of the B2–ZrCo phase and micro-hardness evolution in Zr–Co–Al BMGs via conventional and flash annealing, Journal of Alloys and Compounds 834 (2020) 154230.
[21] K. Yamaguchi, Y.-C. Song, T. Yoshida, K. Itagaki, Thermodynamic investigation of the Cu–Zr system, Journal of Alloys and Compounds 452(1) (2008) 73-79.
[22] H. Peng, M. Li, W. Wang, C.-Z. Wang, K. Ho, Effect of local structures and atomic packing on glass forming ability in Cu x Zr 100− x metallic glasses, Applied Physics Letters 96(2) (2010) 021901.
[23] D. Granata, E. Fischer, J.F. Löffler, Effectiveness of hydrogen microalloying in bulk metallic glass design, Acta Materialia 99 (2015) 415-421.
[24] J. Ding, Y. Cheng, Charge transfer and atomic-level pressure in metallic glasses, Applied Physics Letters 104(5) (2014) 051903.
[25] L. Yang, C.-L. Huang, G.-Q. Guo, Investigation on the atomic structural evolution of as-prepared and annealed ZrCuAl metallic glasses, Journal of Materials Research 27(8) (2012) 1164-1168.
[26] J. Antonowicz, A. Pietnoczka, W. Zalewski, R. Bacewicz, M. Stoica, K. Georgarakis, A. Yavari, Local atomic structure of Zr–Cu and Zr–Cu–Al amorphous alloys investigated by EXAFS method, J. Alloy. Compd. 509 (2011) S34-S37.
[27] S. Achache, F. Sanchette, Effect of Tantalum Addition on Properties of Cu–Zr–Based Thin Film Metallic Glasses (TFMGs), Coatings 10(6) (2020) 515.
[28] Q. Sun, D.M. Miskovic, M. Ferry, Probing the formation of ultrastable metallic glass from structural heterogeneity, Journal of Materials Science & Technology 104 (2022) 214-223.
[29] Y. Sun, C. Cao, K. Huang, N. Zhao, L. Gu, D. Zheng, W. Wang, Understanding glass-forming ability through sluggish crystallization of atomically thin metallic glassy films, Appl. Phys. Lett. 105(5) (2014) 051901.
[30] I. Miccoli, F. Edler, H. Pfnür, C. Tegenkamp, The 100th anniversary of the four-point probe technique: the role of probe geometries in isotropic and anisotropic systems, Journal of Physics: Condensed Matter 27(22) (2015) 223201.
[31] M. Apreutesei, P. Djemia, L. Belliard, G. Abadias, C. Esnouf, A. Billard, P. Steyer, Structural-elastic relationships of Zr-TL (TL = Cu, Co, Ni) thin films metallic glasses, Journal of Alloys and Compounds 707 (2017) 126-131.
[32] X. Li, B. Bhushan, A review of nanoindentation continuous stiffness measurement technique and its applications, Materials characterization 48(1) (2002) 11-36.

[33] W.C. Oliver, G.M. Pharr, An improved technique for determining hardness and elastic modulus using load and displacement sensing indentation experiments, Journal of Materials Research 7(6) (2011) 1564-1583.
[34] D. Pan, A. Inoue, T. Sakurai, M. Chen, Experimental characterization of shear transformation zones for plastic flow of bulk metallic glasses, Proceedings of the National Academy of Sciences 105(39) (2008) 14769-14772.
[35] M. Ghidelli, S. Gravier, J.J. Blandin, P. Djemia, F. Mompiou, G. Abadias, J.P. Raskin, T. Pardoen, Extrinsic mechanical size effects in thin ZrNi metallic glass films, Acta Materialia 90 (2015) 232-241.
[36] C.H. Li, R. Dedoncker, L.W. Li, F. Sedghgooya, F. Zighem, V. Ji, D. Depla, P. Djemia, D. Faurie, Mechanical properties of CoCrCuFeNi multi-principal element alloy thin films on Kapton substrates, Surface and Coatings Technology 402 (2020) 126474.
[37] G. Kresse, J. Furthmüller, Efficient iterative schemes for ab initio total-energy calculations using a plane-wave basis set, Physical Review B 54(16) (1996) 11169.
[38] Y. Le Page, P. Saxe, Symmetry-general least-squares extraction of elastic data for strained materials fromab initiocalculations of stress, Physical Review B 65(10) (2002).
[39] A. Stukowski, Visualization and analysis of atomistic simulation data with OVITO–the Open Visualization Tool, Modelling and Simulation in Materials Science and Engineering 18(1) (2010) 015012.
[40] G. Guo, Quasi-Icosahedral Clusters in Zr-Based Metallic Glasses, Metals 10(9) (2020) 1135.
[41] M. Ghidelli, S. Gravier, J.-J. Blandin, J.-P. Raskin, F. Lani, T. Pardoen, Size-dependent failure mechanisms in ZrNi thin metallic glass films, Scripta Materialia 89 (2014) 9-12.
[42] M. Apreutesei, C. Esnouf, A. Billard, P. Steyer, Impact of local nanocrystallization on mechanical properties in the Zr-59 at.% Cu metallic glass thin film, Materials & Design 108 (2016) 8-12.
[43] N. Mattern, P. Jóvári, I. Kaban, S. Gruner, A. Elsner, V. Kokotin, H. Franz, B. Beuneu, J. Eckert, Short-range order of Cu–Zr metallic glasses, Journal of Alloys and Compounds 485(1-2) (2009) 163-169.
[44] P. Luo, F. Zhu, Y.M. Lv, Z. Lu, L.Q. Shen, R. Zhao, Y.T. Sun, G.B.M. Vaughan, M. di Michiel, B. Ruta, H.Y. Bai, W.H. Wang, Microscopic Structural Evolution during Ultrastable Metallic Glass Formation, ACS Appl Mater Interfaces 13(33) (2021) 40098-40105.
[45] C. Han, W. Yang, Y. Lan, M. Sun, Al addition on the short and medium range order of CuZrAl metallic glasses, Physica B: Condensed Matter 619 (2021) 413237.
[46] G.B. Bokas, L. Zhao, D. Morgan, I. Szlufarska, Increased stability of CuZrAl metallic glasses prepared by physical vapor deposition, Journal of Alloys and Compounds 728 (2017) 1110-1115.
[47] N. Barekar, S. Pauly, R. Kumar, U. Kühn, B. Dhindaw, J. Eckert, Structure–property relations in bulk metallic Cu–Zr–Al alloys, Mater. Sci. Eng. A 527(21-22) (2010) 5867-5872.
[48] A. Guinier, X-ray diffraction in crystals, imperfect crystals, and amorphous bodies, Courier Corporation1994.
[49] J. Dąbrowa, L. Perriere, M. Stygar, W. Kucza, Ł. Klita, M. Danielewski, Oxidation Behavior of Zr43Cu45Al12 Bulk Metallic Glass at 400-525 °C in Air Atmosphere, Journal of Materials Engineering and Performance 24(12) (2015) 4863-4869.
[50] S. Haratian, F. Niessen, F.B. Grumsen, M.J.B. Nancarrow, E.V. Pereloma, M. Villa, T.L. Christiansen, M.A.J. Somers, Strain, stress and stress relaxation in oxidized ZrCuAl-based bulk metallic glass, Acta Materialia 200 (2020) 674-685.
[51] T.L. Cheung, C.H. Shek, Thermal and mechanical properties of Cu–Zr–Al bulk metallic glasses, Journal of Alloys and Compounds 434-435 (2007) 71-74.
[52] Q. Sun, D.M. Miskovic, K. Laws, H. Kong, X. Geng, M. Ferry, Transition towards ultrastable metallic glasses in Zr-based thin films, Applied Surface Science 533 (2020) 147453.
[53] B. Sarac, A. Bernasconi, J. Wright, M. Stoica, F. Spieckermann, M. Mühlbacher, J. Keckes, X. Bian, G. Wang, J. Eckert, Structural modifications in sub-Tg annealed CuZr-based metallic glass, Materials Science and Engineering: A 707 (2017) 245-252.
[54] M. Apreutesei, A. Billard, P. Steyer, Crystallization and hardening of Zr-40at.% Cu thin film metallic glass: Effects of isothermal annealing, Materials & Design 86 (2015) 555-563.

[55] S. Liu, J. Ge, H. Ying, C. Lu, D. Ma, X.-L. Wang, X. Zuo, Y. Ren, T. Feng, J. Shen, H. Hahn, S. Lan, In Situ Scattering Studies of Crystallization Kinetics in a Phase-Separated Zr–Cu–Fe–Al Bulk Metallic Glass, Acta Metallurgica Sinica (English Letters) 35(1) (2021) 103-114.
[56] A.J. Kailath, K. Dutta, T.C. Alex, A. Mitra, Crystallization Study of Cu56Zr7Ti37 Metallic Glass by Electrical Resistivity Measurement, Journal of Materials Science & Technology 27(3) (2011) 275-279.
[57] R. Morel, Y. Huai, R.W. Cochrane, Resistivity and Hall effect in sputtered NiZr metallic glasses, Journal of Applied Physics 64(10) (1988) 5462-5464.
[58] N. Mattern, U. Kühn, H. Hermann, S. Roth, H. Vinzelberg, J. Eckert, Thermal behavior and glass transition of Zr-based bulk metallic glasses, Materials Science and Engineering: A 375-377 (2004) 351-354.
[59] Y.P. Deng, Y.F. Guan, J.D. Fowlkes, S.Q. Wen, F.X. Liu, G.M. Pharr, P.K. Liaw, C.T. Liu, P.D. Rack, A combinatorial thin film sputtering approach for synthesizing and characterizing ternary ZrCuAl metallic glasses, Intermetallics 15(9) (2007) 1208-1216.
[60] M. Zhang, T. Huang, J. Zhang, L. Deng, P. Gong, X. Wang, Influence of Oxidation on Structure, Performance, and Application of Metallic Glasses, Adv Mater 34(52) (2022) e2110365.
[61] M. Apreutesei, P. Steyer, A. Billard, L. Joly-Pottuz, C. Esnouf, Zr–Cu thin film metallic glasses: An assessment of the thermal stability and phases' transformation mechanisms, Journal of Alloys and Compounds 619 (2015) 284-292.
[62] S.V. Madge, D.V. Louzguine-Luzgin, J.J. Lewandowski, A.L. Greer, Toughness, extrinsic effects and Poisson's ratio of bulk metallic glasses, Acta Materialia 60(12) (2012) 4800-4809.
[63] C. Pallier, P. Djemia, D. Fournier, L. Belliard, J. Lu, F. Eriksson, P. Eklund, G. Greczynski, A. le Febvrier, Thermal, electrical, and mechanical properties of hard nitrogen-alloyed Cr thin films deposited by magnetron sputtering, Surface and Coatings Technology 441 (2022) 128575.
[64] X. Ma, X. Bian, N. Zhang, R. Liu, X. Chen, K. Sun, Y. Jia, Q. Wang, G. Wang, Effect of structural heterogeneity on work-hardening behavior of metallic glass thin film, Journal of Alloys and Compounds 913 (2022) 165299.
[65] Y. Ma, G.J. Peng, W.F. Jiang, H. Chen, T.H. Zhang, Nanoindentation study on shear transformation zone in a CuZrAl metallic glassy film with different thickness, Journal of Non-Crystalline Solids 442 (2016) 67-72.
[66] Q. Sun, Development and Characterization of Zr-based Ultrastable Metallic Glasses, UNSW Sydney, 2021.
[67] S. Frank, U.A. Handge, S. Olliges, R. Spolenak, The relationship between thin film fragmentation and buckle formation: Synchrotron-based in situ studies and two-dimensional stress analysis, Acta Materialia 57(5) (2009) 1442-1453.
[68] Y.Q. Cheng, A.J. Cao, H.W. Sheng, E. Ma, Local order influences initiation of plastic flow in metallic glass: Effects of alloy composition and sample cooling history, Acta Materialia 56(18) (2008) 5263-5275.
[69] M. Jawaid, Y. Dang, L. Wang, Q. Fan, E.-R. Kenawy, Relation of Structure, Composition and Glass Forming Ability in Zr-Cu Binary Amorphous Alloys, MATEC Web of Conferences 67 (2016) 03010.
[70] M.H. Abbasi, S.G. Shabestari, R. Tavakoli, On the glass-forming ability of (Zr0.5Cu0.5)100−xAlx ternary alloys: A molecular dynamics study, Materials Today Communications 31 (2022) 103474.